2016

Transient Experimental and 3D-FSI Investigation of Flapper Valve Dynamics for Refrigerant Compressors

Nicholas Carsten Lemke
TU Braunschweig, Germany, n.lemke@tu-bs.de

Michael König
Volkswagen AG, Germany, michael.koenig3@volkswagen.de

Jakob Hennig
Volkswagen AG, Germany, jakob.hennig@volkswagen.de

Sven Försterling
TU Braunschweig, Germany, s.foersterling@tlk-thermo.de

Jürgen Köhler
TU Braunschweig, Germany, juergen.koehler@tu-bs.de

Transient Experimental and 3D-FSI Investigation of Flapper Valve Dynamics for Refrigerant Compressors

Nicholas C. LEMKE[1]*, Michael KÖNIG[2], Jakob HENNIG[2], Sven FÖRSTERLING[1], Jürgen KÖHLER[1]

[1] Institute of Thermodynamics, Technical University of Braunschweig,
38106 Braunschweig, Niedersachsen, Germany
E-mail: n.lemke@tu-bs.de, j.koehler@tu-bs.de

[2] Volkswagen AG, Component Development,
38231 Salzgitter, Niedersachsen, Germany
E-mail: michael.koenig3@volkswagen.de, jakob.hennig@volkswagen.de

* Corresponding Author

ABSTRACT

The design of the valves for refrigerant compressors has a distinct influence on the efficiency of the refrigeration cycle. In order to predict the valve behavior for compressor optimization, flow characteristics and valve system dynamics are key factors. State of the art valve model approaches have to date ignored the retainer deflection and the influence of contact effects on fluid-structure interaction behavior. With this fact in mind, experimental valve lift investigations by means of laser vibrometry measurements were performed. In order to determine the dynamic flapper valve characteristics, oscillation frequency analyses for free oscillation of the flapper valve were carried out and compared to a FEA modal analysis.
Additionally this paper presents an extended three-dimensional numerical discharge valve model containing a fully-coupled fluid-structure interaction (FSI) approach. The two-way mechanical coupling is carried out by a commercial CFD code combined with a commercial FEM package. The numerical results of a 1D and the 3D-FSI model are validated using the presented experimental transient results. The numerical 3D-FSI results show good agreement with the experimental results with respect to the obtained oscillation frequencies. The 1D model allows error estimation of the mass flow considering retainer deflection. Neglecting the retainer deflection yields a maximum error of four percent for experimental boundary conditions.

1. INTRODUCTION

Pressure actuated reed valves (flapper valves) are widely used in the suction and discharge part of refrigerant compressors. Self-acting reed valves basically respond to pressure differences across the valve. Due to in-flow and out-flow characteristics, geometrical and momentum effects reed valves cause 'valve flutter' and over-compression losses. Valve flutter describes the multiple opening and closing process during suction and discharge process through reed valves (Dhar *et al.*, 2014, Min *et al.*, 2014). The efficiency of reciprocating compressors is significantly influenced by the valve performance. General replacement of synthetic refrigerants by natural refrigerants considering high system absolute pressures – especially CO_2 (R744) – requires increased performance and reliability improvement of reed valves for both suction and discharge port. For that reason valve dynamics need to be deeply studied for various operating conditions. The present study employs experimental as well as 1D and 3D-FSI modeling for oil-free valve dynamics investigations. The study is particularly focusing on the extension of reed valve dynamics by retainer deflection and contact effects. The schematics of a flapper suction valve and flapper discharge valve with retainer can be seen in Figure 1. The flapper valve consists of a valve plate comprising the bore for refrigerant suction and discharge. The reed is excited by external pressure load. During the suction and discharge process the reed oscillates between the retainer and the valve plate. The discharge reed is clamped between the valve plate and the retainer which restricts to the maximum valve lift $x_{\max}$. For positive pressure differences the refrigerant flows from the bore to the valve, as denoted by the direction of the mass flow $\dot{m}$ (cf. Figure 1). Pressure drop through the valve especially depends on geometrical parameters such as maximum reed lift and bore diameter. Both

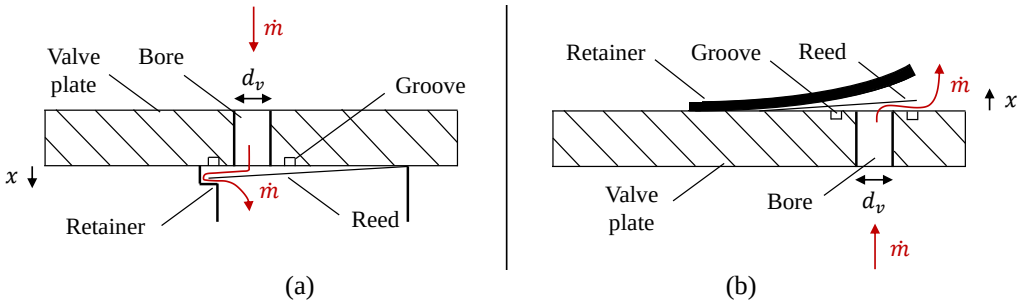

Figure 1: Schematic of flapper valve, (a) suction part, (b) discharge part

parameters significantly limit the flow area for the refrigerant in- and outflow between valve plate and reed. Maximum mechanical reed lifts of 1.05 mm for the suction valve and 0.388 mm and 0.642 mm for the discharge valve were allowed (measurement data at the axis of the bore). Both suction and discharge bore diameter have not been varied. Suction and discharge reeds with different thickness values (0.2 mm, 0.25 mm and 0.3 mm) have been investigated. A coated reed of 0.2 mm is additionally investigated. The coating is applied at both sides of the reed.

2. EXPERIMENTAL SETUP

For experimental investigation of a suction and discharge valve an experimental device with a reproduced reed valve from a refrigerant compressor was designed, operating in dry, oil-free conditions. Figure 2 shows the schematic of the test rig.

The test rig comprises a 300 bar storage nitrogen bottle. The decompression pressure is controlled by a manually actuated decompression valve. The valve pressure is set electronically by a LabVIEW-controlled solenoid valve. The outflow is detected by a Coriolis mass flow sensor. The decompression pressure (pressure transmitter) and the valve pressure (pressure transducer) as well as the valve temperature (thermocouple) are synchronously recorded. Constant outflow or single short pressure surges generated by the solenoid valve represent two different operating conditions which can be investigated at flapper valve test rig. The valve outflow is drained to the environment. For the reduction of valve unit vibrations a massive test housing was mounted around the valve. The valve lift is detected by a laser vibrometer orthogonally aligned on the reed for optimum signal quality. Figure 3 shows a schematic of the suction and discharge reed valve comprising a retainer bore for laser vibrometric lift measurements.

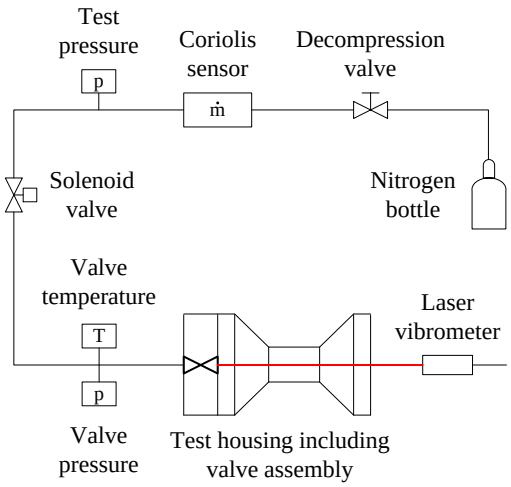

Figure 2: Schematic of test rig for dynamic investigation of flapper valves

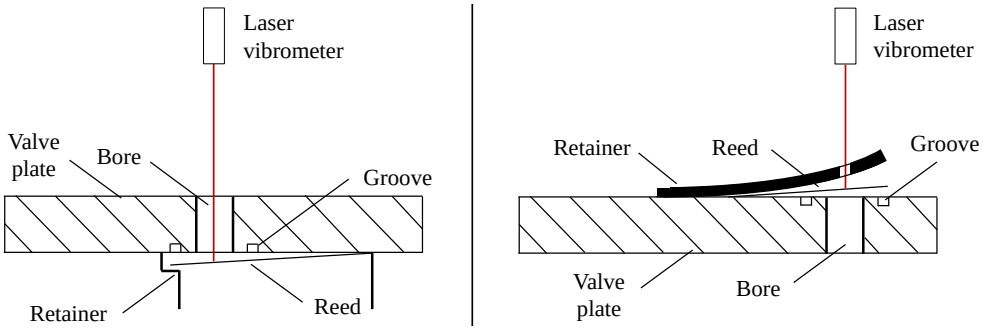

Figure 3: Schematic of reed valve with optical lift measurement, (a) suction valve, (b) discharge valve

3. NUMERICAL MODELING

3.1 1D valve dynamics and mass flow

The reduced model for a reed valve considers inertia, damping and stiffness effects on the one side and the pressure difference Δp as driving force on the other side of the force balance acting on the reed. The valve lift dynamics are described by a spring-mass system in the following general form as a one degree of freedom model:

$$F_{\mathrm{p}}(t) = m\ddot{x}_{\mathrm{v}} + b\dot{x}_{\mathrm{v}} + cx_{\mathrm{v}} = A_{\mathrm{eff}} \cdot \Delta p. \tag{1}$$

Where, m is the effective substitute valve mass, b is the damping factor and c is the substitute stiffness. The effective force area is considered as:

$$A_{\mathrm{eff}} = A_{\mathrm{geo}} \cdot c_{\mathrm{pv}}. \tag{2}$$

A_{geo} is the geometrical force area (equal to the bore area) corrected by an empirical force coefficient c_{pv}. The underlying equations and valve parameters are widely summarized by Touber (1976) and extended by Boeswirth (1994) and Baumgart (2010). Within the applied 1D model, the different valve parameters are calculated dependent on the valve geometry and for each discrete value of the valve displacement x_{v}. The resulting explicit non-linear second-order ordinary differential equation which is numerically solved using an implicit Runge-Kutta formula for stiff systems is derived as follows:

$$\frac{\mathrm{d}^2 x_{\mathrm{v}}}{\mathrm{d}t^2} = \frac{1}{m(x_{\mathrm{v}})}\left[c_{\mathrm{pv}}(x_{\mathrm{v}}) \cdot \frac{\pi}{4} \cdot d_{\mathrm{v}}^2 \cdot \Delta p - F_{\mathrm{s}}(x_{\mathrm{v}}) - b(x_{\mathrm{v}})\frac{\mathrm{d}x_{\mathrm{v}}}{\mathrm{d}t}\right]. \tag{3}$$

The normalized values ($\Phi^* = \Phi/\Phi_{\max}$) of the valve parameters m, F_{s}, b and c_{pv} of the 1D valve model depending on the normalized valve lift ($x^* = x/x_{\max}$) are given in Figure 4 for the investigated discharge valve. As soon as the valve interacts with the retainer and begins to align with the retainer shape ($x^* \approx 0.68$), the substitute valve mass m begins varying and the valve spring force F_{s} changes from linear to non-linear behavior. The damping coefficient b has local maximum values at $x^* \approx 0$ and $x^* \approx 1$ due to fluid damping effects at the valve seat and the retainer, whereby the damping effect at the valve seat is smaller. The pressure coefficient c_{pv} slightly increases due to decreasing pressure loss across the valve during the opening process. Since oil-free conditions are investigated, no additional adhesive effect is considered.

The resulting mass flow $\dot{m}_{\mathrm{v}}$ through the valve is calculated using a semi-empiric approach based on the Bernoulli equation for incompressible, frictionless, stationary and horizontal flows, corrected by the flow coefficient α and the expansion coefficient ε:

$$\dot{m}_{\mathrm{v}}(t) = A_{\mathrm{flow}}(x_{\mathrm{v}}) \cdot \alpha(x_{\mathrm{v}}) \cdot \epsilon(p_0, p_1) \cdot \sqrt{2\Delta p \cdot \rho_0}. \tag{4}$$

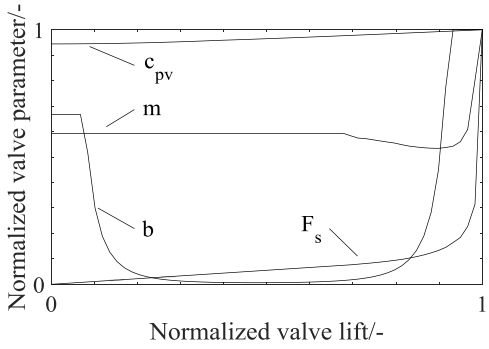

Figure 4: Valve lift dependent parameters of the 1D valve model (discharge valve, 0.25 mm valve thickness, 0.642 mm maximum theoretical valve lift)

Where, A_{flow} is the geometrical flow area, formed by the smallest shell surface between the valve seat and the valve. The retainer deflection is taken into account by a superposition approach. The valve displacement x_{v} calculated by solving Equation (3) is superposed by the retainer deflection x_{ret} leading to the total displacement x_{tot}:

$$x_{\mathrm{tot}} = x_{\mathrm{v}} + x_{\mathrm{ret}}. \tag{5}$$

The retainer deflection x_{ret} is calculated assuming a linear-elastic material behavior, considering the pressure force F_{p} acting on the valve reed (cf. Equations (1) and (3)). The substitute stiffness of the retainer is determined experimentally in the present study.

$$x_{\mathrm{ret}} = \frac{F_{\mathrm{p}}}{k_{\mathrm{ret}}} = \frac{c_{\mathrm{pv}}(x_{\mathrm{v}}) \cdot \frac{\pi}{4} \cdot d_{\mathrm{v}}^2 \cdot \Delta p}{k_{\mathrm{ret}}} \tag{6}$$

3.2 Fully-coupled 3D-FSI valve model

For a deeper understanding of the complex valve flow phenomena in consideration of the valve movement and deformation, a fully-coupled three-dimensional fluid-structure interaction (FSI) model for the investigated discharge valve is developed. The results are compared to the 1D results and the test rig measurements. The FSI model comprises the mechanical parts of the test housing (cf. Figure 2) and its connection to the test rig. The two-way mechanical coupling is realized by a commercial CFD code (STAR-CCM+, version 10.06) combined with a commercial FEA package (Abaqus, version 6.14). The pressure and stress data (CFD) and the geometrical displacement (FEA) are interchanged at any discrete time step. The 3D computational CFD grid consists of a fixed background mesh (3.5 M grid cells) including the boundary definitions and an overset mesh (1.9 M grid cells) which is morphed based on the displacement of the valve surface coupled with the FEA solver. The overset grid approach allows for modelling zero-gap configurations, especially if the valve is closed (cf. Figure 5 (a)) or in contact with the retainer. The CFD setup contains compressibility (ideal gas formulation) and turbulence modeling (SST k-omega model). The solution scheme is coupled for pressure and velocity and second-order implicit unsteady in time with a time step of $1.5 \cdot 10^{-5}$ s. In order to improve the numerical stability, the measured pressure data upstream of the valve have been smoothed and set up as inlet pressure boundary condition. Ambient pressure is set at the outlet boundary condition.

The FEA model consists of three parts: The reed, the retainer and the valve seat (cf. Figure 5 (b)), each of them consisting of about 3000 C3D20R-elements. All parts are modeled as solid bodies in order to be able to handle the contact events. Within the FEA model, the retainer is deformable, influencing the the valve lift. The CFD model, however, solely considers the movement of the reed (the retainer is assumed to have no influence on the flow field).

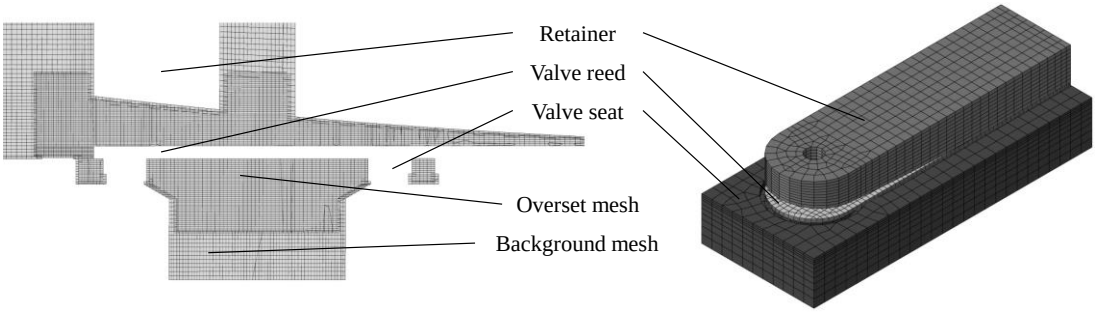

Figure 5: (a) Section of the computational CFD grid and (b) structural FEA model combinded for FSI coupling for the discharge valve

4. RESULTS AND DISCUSSION

4.1 Frequency analyses

In a first step external pressure surge measurements of oscillation frequency for suction and discharge valve were carried out. For determining oscillation frequencies the flapper valves are manually actuated while the valve lift is recorded. Figure 6 shows the absolute lift for the discharge valve over time, starting with maximum deflection amplitude of about 1 mm. Based on the measurements for the manual mechanical excitation, a frequency analysis was carried out.

Table 1 shows the identified oscillation frequency for the suction and discharge valves by varying reed thicknesses. The frequency values increase with higher thicknesses of the reed. For a non-damped mass-spring system increased reed stiffness leads to higher frequencies of the reed. Particularly the comparison of 0.20 mm and 0.20 (coated) for the suction valve and discharge valve, respectively, indicates a low effect of the coating on the natural frequency, compared to the influence of the effective metal valve thickness. This is confirmed by similar oscillation frequencies of the coated and non-coated 0.20 mm reeds although the coated valve has a ten percent higher absolute mass. A FEA modal analysis for the discharge valve with a thickness of 0.25 mm (cf. Figure 5 (b)) for free oscillation conditions yielded a natural frequency of 400 Hz for the first mode, which is about nine percent higher than the measured oscillation frequency (366 Hz). Although the FEA modal analysis does not consider physical fluid friction and damping due to ambient fluid the experimental and simulation results for the free valve oscillation fit well. The FEA modal analysis thus can be applied to predict natural frequency for the reed (cf. Section 4.2 (i)).

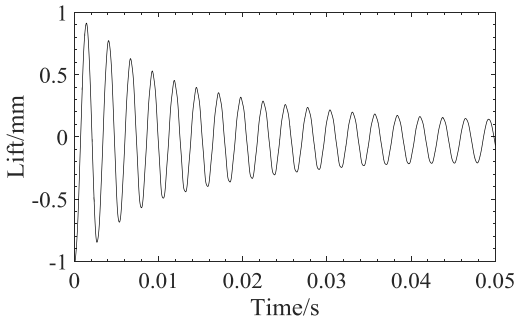

Figure 6: Free valve oscillation due to manual mechanical excitation (discharge reed valve thickness 0.25 mm)

Table 1: Mean oscillation frequency of reproduced suction and discharge valve

Reed thickness/mm	**Oscillation frequency/Hz**	
	Suction valve	Discharge valve
0.20	538	292
0.20 (coated)	557	274
0.25	695	366
0.30	765	449

4.2 Lift measurements

For further studies on valve dynamics during opening and closing events, lift measurements for short pressure surges for approximately 0.1 s were carried out. Figure 7 (a) shows the discharge reed lift and the retainer lift for a reed thickness of 0.25 mm with a maximum theoretical reed lift of 0.642 mm at the valve bore axis determined by the retainer. The reed lift and the retainer lift were recorded for consecutive measurements. The identified oscillation frequencies for the reed and the retainer are shown in Figure 7 (b) for sections (i), (ii) and (v) depicted in Figure 7 (a). A test pressure of 60 bar was applied. Due to throttle effects of the solenoid and the decompression valve (cf. Figure 2) the maximum absolute pressure upstream of the valve is significantly lower than the test pressure. The actual pressure difference between upstream pressure of the reed valve and ambient pressure is 7.6, 3.4, 1.4 and 0.47, respectively, for 120, 60, 30 and 10 bar test pressure. The evaluation of the following experimental results focusses on the discharge reed valve.

When the pressure surge upstream of the valve is applied at 0.006 s the opening process of the valve starts. The opening and closing process can be subdivided into six sections. Figure 7 illustrates the valve behavior for any section.

(i) The opening process of the valve starts as soon as the pressure signal is increasing. The reed valve oscillates between retainer and valve plate with decreasing oscillation amplitude. The reed is bent around the retainer resulting in smaller bending lengths for the reed. A retroactive effect between the reed and the retainer can be observed resulting in similar oscillation frequencies of the reed and the retainer. The oscillation frequencies of the reed and the retainer vary from about 800 Hz to 2000 Hz. The oscillation frequency for the first opening interval is close to the natural frequency from an FEA modal analysis of 829 Hz (first mode). The FEA analysis is carried out for the clamped reed. Since the retainer reduces the oscillation length of the reed (cf. Figure 5 (b)), the natural frequency for the mounted valve is higher than the free oscillation frequency of the total reed length (cf. Section 4.1).

(ii) The lift as well as the oscillation frequencies of the reed and the retainer are steadily increasing. The reed lift results in an interaction between reed, retainer and pressure with increasing amplitude of the lift, compatible with the behavior of a pressure forced oscillation of a coupled spring mass system. The obtained frequencies are determined by the oscillation length of the reed resulting from the valve lift.

(iii) The oscillation amplitude of the coupled system is approaching zero. A minimum bending length of the reed is obtained. At the end of section (iii) a maximum lift height is obtained when valve pressure gains a maximum value indicating the retainer deflection. No interaction between retainer and pressure is observed.

(iv) The valve pressure decreases, whereas the reed remains attached to the retainer. In consequence the reed valve and the retainer lift decrease while oscillation amplitude is low. At the end of section (iv) the reed begins again to interact with the retainer resulting in similar oscillation frequencies.

(v) The reed continuously detaches from the retainer. The reed oscillates with increasing amplitude while oscillation frequency is decreasing to values comparable to the end of section (i). Again, an interaction between reed, retainer and pressure is observed, however the retroactive effect is not as significant as in section (ii).

(vi) The reed completely loses from the retainer back to its initial position on the valve seat. The valve pressure drops to initial ambient pressure of around 1 bar.

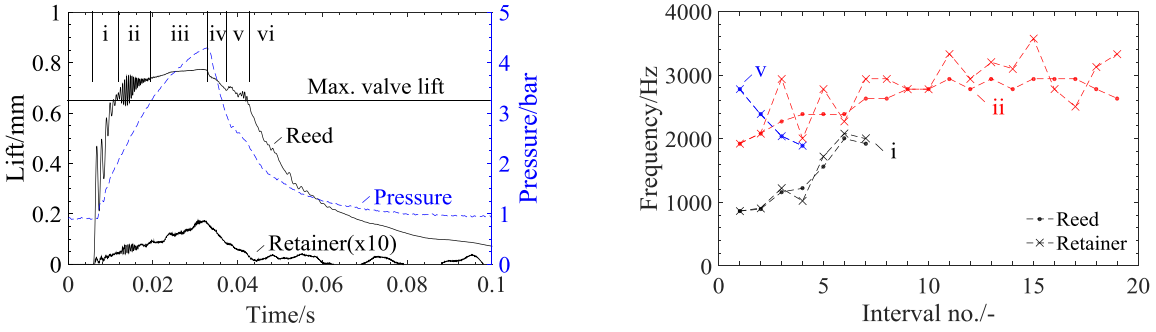

(a) (b)

Figure 7: (a) Discharge valve lift and retainer lift (factor 10) with absolute pressure plot, (b) Frequency analysis for reed and retainer (valve thickness 0.25 mm, 0.642 mm retainer, 60 bar test pressure)

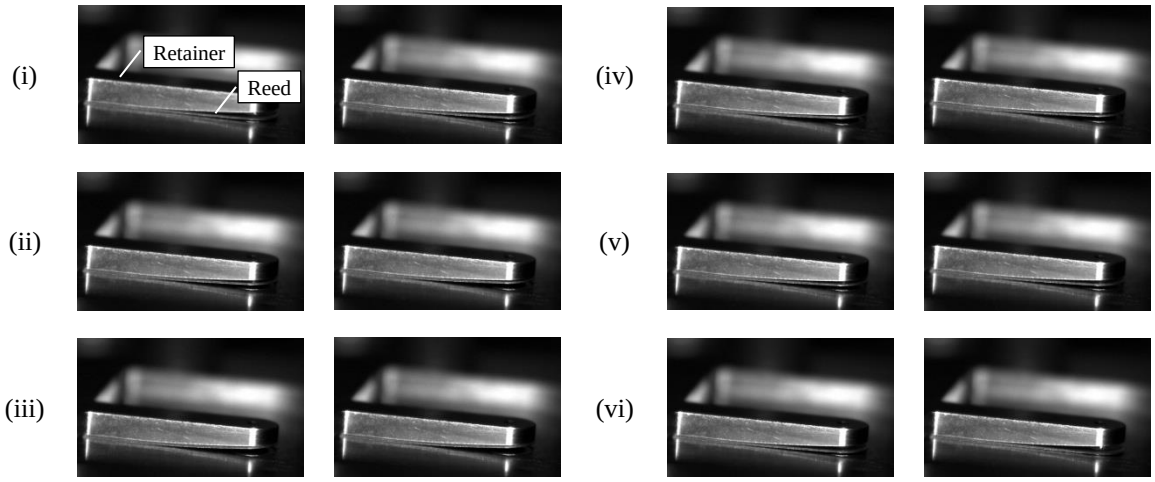

Figure 8: High speed video analysis for opening and closing process of discharge valve; left: beginning of section; right: end of section (valve thickness 0.25 mm, 0.642 mm retainer, 60 bar test pressure)

For the opening process in sections (i) and (ii) the oscillation frequencies of the reed and the retainer could clearly be determined. The oscillation frequencies of the reed and the retainer show similar values for the entire opening process due to interaction, cf. Figure 7 (b). Sections (iii) and (vi) do not show significant oscillations for a frequency analysis. For the closing process in section (v) the oscillation frequencies could again clearly be determined while oscillation frequencies are equal resulting from the reed and the retainer interaction. Figure 8 illustrates the reed lift for each section. The general opening and closing characteristics for varied discharge reed thicknesses, retainer geometries and varied suction reed thicknesses are similar. Due to possible geometrical laser vibrometer misalignment the measured valve lift values exceed the theoretical maximum valve lift, cf. Figure 7 (a). The maximum valve lift uncertainty is identified to be 20 % and can be adjusted by a scaling factor with the help of the numerical results, cf. Section 4.3. The general reproducibility error in lift measurement is identified to be one percent.
Figure 9 shows selected reed valve lift and pressure plots for different test pressure acting on discharge reed valve with 0.25 mm reed thickness. The valve pressure is increasing along with increasing test pressure. The valve lift measurements show longer open periods for increasing test pressure. The maximum valve lift is obtained for a maximum test pressure of 120 bar. The test pressures of 10 and 30 bar show continuous oscillation for the opening process. Sections (iii) and (iv) are not observed for 10 and 30 bar test pressure because the reed is not in complete contact with the retainer. For 10 bar even section (ii) is not present as a result of small lift amplitude. Resonance oscillation for the coupled reed and retainer spring mass system is distinct for 60 bar testing pressure. Oscillation amplitudes of more than 0.1 mm can be observed where no contact between reed and retainer is achieved. A higher valve lift is measured for 120 bar test pressure compared to 60 bar test pressure although both measurements show contact

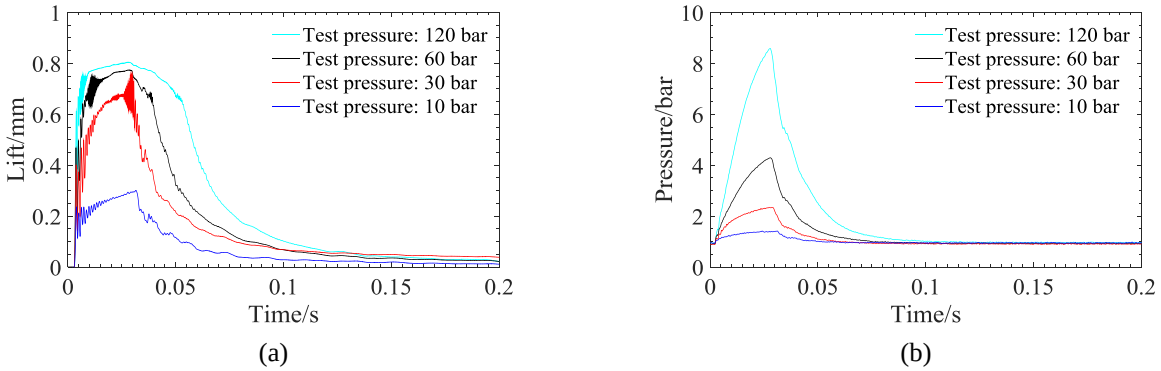

Figure 9: (a) Discharge valve lift and (b) pressure plot for different test pressures of 10, 30, 60 and 120 bar (valve thickness 0.25 mm, 0.642 mm retainer)

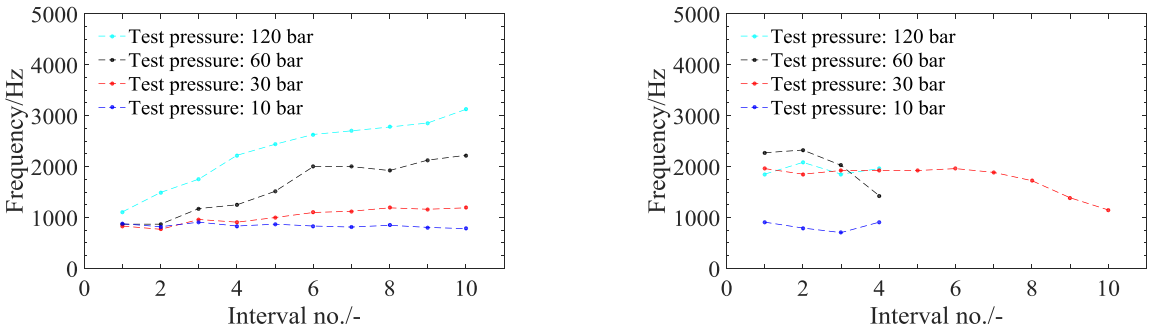

Figure 10: Frequency analysis of discharge valve lift: (a) opening process (cf. Figure 7, section (i)) and (b) closing process (cf. Figure 7, section (v)) (valve thickness 0.25 mm, 0.642 mm retainer)

behavior between valve and retainer. This demonstrates the effect of the retainer deflection on the total valve lift. Due to a higher density of nitrogen at higher test pressures, a higher mass of nitrogen needs to be expanded through the valve, resulting in a longer open period.

Figure 10 shows a frequency analyses for the discharge valve lift during opening and closing processes for different test pressures as far as oscillation lift maxima and minima can be determined. The frequency analyses of the valve lift measurements for any test pressure show similar frequencies for the first interval when opening (about 700 to 1100 Hz) and closing (about 1700 to 2300 Hz) for investigated test pressures from 10 to 120 bar. Further on the frequencies for the opening process show a similar progression for all test pressures as the frequency increases over the interval number up to 3000 Hz for 120 bar test pressure. For higher test pressures the frequency seems to be less damped. In contrast to the opening process the frequencies for the closing process decrease over the interval number from a frequency of 2000 Hz to a frequency of 1000 Hz for 30 bar test pressure; however the number of intervals is very low for 10, 60 and 120 bar test pressure. The measured frequencies due to pressure surges are significantly higher than measured free oscillation and natural frequencies for the discharge valve (cf. Table 1), caused by the reduced bending length of the clamped reed. In case of 10 bar test pressure, the reed shows lower frequencies, compared to higher test pressures, since it does not fully align with the retainer, cf. Figure 9 (a).

The frequency deviation between pressure surges and free oscillation as well as natural frequency can be explained by two physical facts: The first effect is the interaction between the reed and the retainer which results in a coupled spring-mass system with resonance phenomena and changed oscillation frequencies. The second effect is the interaction between the fluid and the reed which also leads to changed resonances and oscillation frequencies. Both effects can deeper be investigated by employing numerical models, as presented in the following.

4.3 Numerical results

The analysis of the numerical results covers the evaluation of the valve lift over time calculated by the above described 1D/3D-FSI models, see Figure 11. In order to compare them to the experimental results, the experimental lift data are adjusted by a constant scaling factor of 0.83, compensating the above mentioned measuring inaccuracy. The maximum lift is chosen as scaling reference value. The valve lift measurement for 60 bar (cf. Figure 7) is chosen as validation example comprising a representative valve behavior. For the 3D-FSI model, the valve lift in the bore axis has been analyzed. Due to high computational effort the 3D-FSI simulation is stopped after passing the maximum valve lift (at 0.03 s) and analyzed with focus on the valve opening process, as shown in Figure 11 (a). The overall shape of the valve lift fits well for both the 1D and the fully-coupled 3D-FSI model, compared to the scaled experimental data. The 1D model is unable to describe the identified oscillations in section (ii), cf. Figure 7. The 3D-FSI model, however, reproduces a characteristic oscillation behavior in the section of interest, even though the oscillation starts earlier and the calculated amplitude values are lower than the experimental values. The 3D-FSI model shows approximately ten characteristic oscillation intervals. The first oscillation shows a frequency of 1750 Hz, which is about twice the natural frequency of the clamped reed (first mode of FEA modal analysis: 829 Hz), whereas the tenth oscillation frequency is about 2780 Hz. This trend shows a good agreement to the experimentally determined frequencies at section (ii), cf. Figure 7 (b). Once the valve passed the section of distinct interaction of the reed and the retainer both models show good agreement with respect to the total displacement. The retainer deflection is also corresponding to the experimental results.

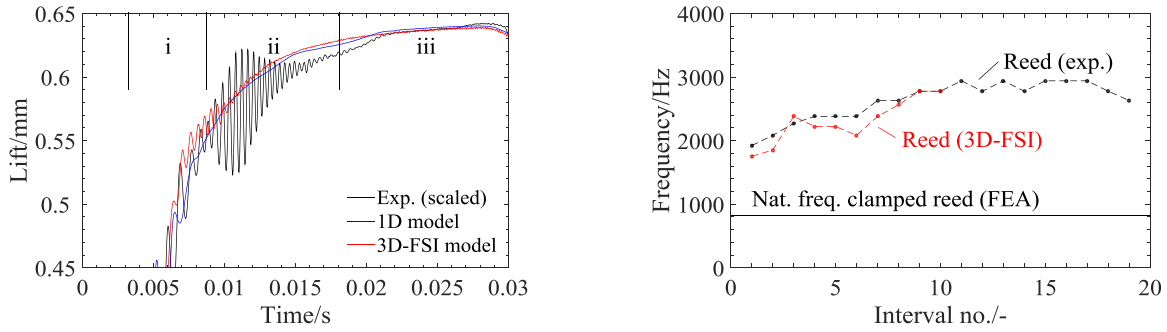

(a) (b)

Figure 11: (a) Calculated valve lift curves of 1D and 3D-FSI model at the opening sections (i) to (iii) and (b) frequency analysis for 3D-FSI lift data at section (ii) compared to experimental data, cf. Figure 7 (valve thickness 0.25 mm, 0.642 mm retainer, 60 bar test pressure)

The evaluation of the influence of the retainer deflection on the total valve lift and the resulting mass flow is carried out based on the 1D valve model for a test pressure of 120 bar (cf. Figure 9 (b)). As shown in Figure 12, the valve displacement x_v does not exceed the maximum theoretical valve lift of 0,642 mm, if the retainer is assumed to be infinite stiff. Taking into account the experimentally obtained retainer stiffness ($k_{ret} = 3.2 \cdot 10^5$ N/m), the retainer deflection x_{ret} achieves a maximum value of 0.024 mm, leading to a maximum total displacement of 0.663 mm. Thus, neglecting the retainer deflection results in a mass flow estimation error, see Equation (4). As illustrated in Figure 12, the maximum difference $\Delta\dot{m}_{v,max}$ between the normalized total mass flow in consideration of the retainer deflection $\dot{m}^*_{tot}$ and the normalized mass flow for a stiff retainer $\dot{m}^*_{stiffRet}$ achieves a value of almost four percent. The integration of the mass flow yields the cumulative mass $m_{v,0.1s}$ which passed the valve due to one pressure surge. For the maximum test pressure of 120 bar, the error $\Delta m_{v,0.1s}$ when neglecting the retainer deflection sums up to 2.2 %-, compared to the cumulative mass considering the retainer deflection. The calculated values for maximum retainer deflection $x_{ret,max}$, maximum mass flow difference $\Delta\dot{m}_{v,max}$ and cumulative mass difference $\Delta m_{v,0.1s}$ are summarized in Table 2. It is evident that the error when neglecting the retainer deflection increases by increasing pressure difference. For lower pressure differences the retainer difference can be neglected.

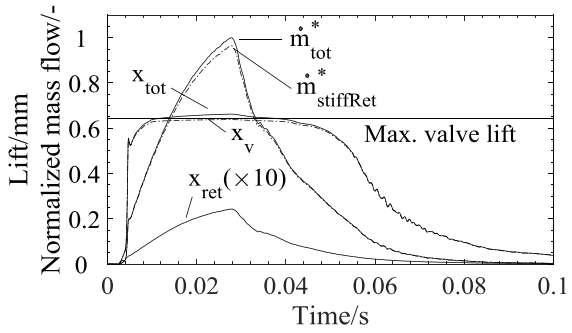

Figure 12: Valve lift and normalized mass flow calculated by the numerical 1D model with and without superposition of retainer deflection (valve thickness 0.25 mm, 0.642 mm retainer, test pressure 120 bar)

Table 2: Error estimation for mass/mass flow calculation at different pressure differences when neglecting the retainer deflection based on the 1D model

Test pressure/bar	**10**	**30**	**60**	**120**
$\Delta p_{v,max}$/bar	0.47	1.4	3.4	7.6
$x_{ret,max}$/mm	0.0014	0.0046	0.011	0.024
$\Delta\dot{m}_{v,max}$/%	0.65	0.67	1.4	3.6
$\Delta m_{v,0.1s}$/%	0.68	0.63	0.98	2.2

6. CONCLUSION

This study focuses on the dynamics of flapper valves for refrigerant compressors by means of laser vibrometry valve lift measurements for various operating conditions. A frequency analysis is carried out for suction and discharge valves with different thicknesses, which allows estimating the free oscillation behavior of a single valve. Further on, lift measurements for the discharge valve-retainer assembly excited by different pressure surges give a deeper understanding of the transient behavior and show distinct interaction and resonance effects between valve and retainer. Analyzing the oscillations of the coupled system shows varying frequencies which cover a range frequency in the order of 1000 Hz to 3000 Hz. Any experimental investigations have been carried out for dry conditions.
Additionally a 1D and a 3D-FSI valve model are presented and evaluated with focus on the valve lift. Compared to the experimental results, the 1D model reproduces well the generic valve lift behavior and mass flow characteristics. However it is incapable of describing the distinct oscillations of the system. The 3D-FSI model shows good agreement to the experimentally obtained oscillation frequencies of the coupled system, especially when valve and retainer begin to interact. To obtain deeper knowledge on the complexity of valve flows, further experimental and numerical investigations considering multiphysics phenomena such as adhesive effects should be carried out.

NOMENCLATURE

A	area	(m^2)	ρ	density	(kg/m^3)
b	damping coefficient	(Ns/m)	Φ*	normalized physical quantity	(–)
c	stiffness	(N/m)			
CFD	computational fluid dynamics				
c_{pv}	pressure coefficient	(–)	**Subscript**		
d	(bore) diameter	(m)	0	upstream value	
F	force	(N)	1	downstream value	
FEA	finite element analysis		eff	effective	
FSI	fluid-structure interaction		geo	geometrical	
k	stiffness	(N/m)	max	maximum value	
m	mass	(kg)	p	pressure	
$\dot{m}$	mass flow	(kg/s)	ret	retainer	
p	pressure	(Pa)	s	spring force	
t	time	(s)	tot	total	
x	lift, displacement	(m)	v	valve	

REFERENCES

Baumgart, R. (2010). *Reduzierung des Kraftstoffverbrauches durch Optimierung von Pkw-Klimaanlagen. Doctoral thesis*. Chemnitz, Germany: Chemnitz University of Technology, Department of Mechanical Engineering.

Boeswirth, L. (1994). *Stroemung und Ventilplattenbewegung in Kolbenverdichterventilen*. Vienna: Self-published.

Dhar, S., Tamma, B., Bhakta, A., Krishna, M. (2014). An approach towards reed valve geometry design. International Compressor Engineering Conference, Purdue University, Indiana, USA, Paper 1144.

Min, B., Noh, K., Yang, J., Choi, G., Kim D. (2014). Prediction of Refrigerant Leakage for Discharge Valve System in a Rolling Piston Compressor. International Compressor Engineering Conference, Purdue University, Indiana, USA, Paper 1464.

Touber, S. (1976): *A Contribution to the Improvement of Compressor Valve Design. Doctoral Thesis.* Delft, Netherlands: Delft University of Technology, Department of Mechanical Engineering.

ACKNOWLEDGEMENT

The authors would like to thank our colleagues at the Volkswagen R&D department, B.Sc. Norman Welz, B.Sc. Maximilian Müller, Dr. Andreas Gitt-Gehrke and Dipl.-Wirtsch.-Ing. Mathias Möller, for their contribution and support to this paper.